INTRODUCTION TO INTRABEAM SCATTERING

A.H. Sørensen
Institute of Physics, University of Aarhus, Denmark

1. PRELUDE

The purpose of the present report is to give an introductory discussion of the influence of internal scattering events on the evolution of the phase-space density of a charged particle beam. This topic is commonly known as intrabeam scattering. To initiate our studies and obtain a background for understanding the specific case of a beam, we consider at first in general the rôle played by collisions in a plasma (an ionized gas).

For a system containing a total of N particles we construct a 6N-dimensional phase space. A continuity argument proves the Liouville theorem, which states that the density in this space remains a constant when measured along phase-space trajectories provided all forces acting are Hamiltonian. It is stressed that interparticle forces, which are indeed Hamiltonian, enter on equal footing with external forces. The multi-dimensional space is very impractical, however, and a reduction to everyday 6-dimensional phase space is requested. In the course of this reduction, problems pop up with the interparticle interactions. They turn out to be separable into a Liouvillian "space-charge" force, associated with the collective action on a given "test particle" of the rest of the gas, and scattering events. The collisions, which add a term to the Liouvillian part of the equation governing the evolution of the distribution function in 6-dimensional phase space, are responsible for relaxation towards equilibrium. Assuming dominance of soft multiple collisions, the Fokker-Planck equation emerges and further introduction of a naïve model for the encounters leads to determination of the friction and diffusion coefficients. To complete the general discussion, we evaluate rates of diffusion for the specific cases of spatially homogeneous plasmas having isotropic and collapsed Maxwellian velocity distributions, respectively.

When we turn to the case of a charged particle beam, the question immediately appears what may be different from the general plasma case? When the average longitudinal motion is transformed away - by working in the "particle frame" moving along the storage ring at the nominal beam velocity - the answer is: very little. Scattering events appear as in the plasma, only the distribution function is given in another set of generalized coordinates $(x_\beta, x'_\beta, \ldots)$ than the usual rectangular ones $(x, p_x, \ldots)$. In the beam case we encounter couplings, for instance between longitudinal and horizontal motion. We shall outline practical calculations, which account for such couplings. Among these we mention the treatment of Piwinski[1] with later improvements [2]. However, instead of going into mathematical details at this point, we choose to show some theoretical results for coasting proton beams obtained by means of existing computer codes. The numerically obtained rates help to single out where the aforementioned couplings are essential for the scattering processes

and where not. Furthermore, the data bring us in a natural way towards a discussion of the possible existence of a set of reduced variables, which would allow for a compact representation of results over a wide range of initial conditions. The question appears, whether we may create some reasonably general and simple curves, which could provide quick and reliable estimates of beam blow-up rates - without the computer? The study of the plasma gives some hints.

2. GENERAL DESCRIPTION

2.1 Liouville in 6N-dimensions

Consider a non-relativistic gas consisting of N interacting charged particles. Most generally, such a system possesses 3N degrees of freedom. A canonical representation therefore requires 3N generalized coordinates, q_i, and 3N conjugate momenta, p_i. In 6N-dimensional phase space $(q_1, \ldots, q_{3N}, p_1, \ldots, p_{3N})$, the full system is represented by a single point at a given time, Fig. 1a. Often, for q_i we shall take the rectangular coordinates (x,y,z) of the positions of the individual particles and for p_i the corresponding linear momenta. In this case the coordinates 3n-2, 3n-1, 3n of the phase-space point define the position of particle number n whereas the coordinates 3(N+n)-2, 3(N+n)-1, 3(N+n) fix the momentum of that particle. In general, the conjugate momenta are obtained from the Lagrangian, L, according to the relation

$$p_i = \partial L/\partial \dot{q}_i \ , \qquad L(q,\dot{q},t) \equiv T - U \ . \tag{1}$$

Here the dot represents the total time derivative d/dt and T denotes the kinetic energy of the system. The quantity U is the potential energy. As an example, if we choose the q's as the spherical coordinates (r,θ,φ) to the individual positions of the particles, one third of the p_i's correspond to the radial momenta of the particles, the remaining p_i's reflect the φ- and θ-components of the angular momenta.

To determine the path followed in time by the phase-space point, Fig. 1a, we need some equations of motion. These may be expressed as differential relations involving the Lagrangian. Alternatively, one may introduce a Hamiltonian,

$$H(q,p,t) \equiv \sum_i p_i \dot{q}_i - L \ . \tag{2}$$

We recall that in case only time-independent conservative forces are acting, H is a constant of motion, the total energy. In general, the total force active divides into a conservative, or Hamiltonian, part and a non-conservative contribution. The former corresponds to the part of the force which is derivable from a potential U, where $U=U(q,\dot{q},t)$ appears as a sum of the usual scalar potential and a term accounting for electromagnetic forces on moving charges [3]. The non-Hamiltonian part Q_i represents friction and inelastic processes. By means of the Hamiltonian, the 6N equations of motion then take the form

$$\dot{p}_i = -\frac{\partial H}{\partial q_i} + Q_i \ , \qquad \dot{q}_i = \frac{\partial H}{\partial p_i} \ . \tag{3}$$

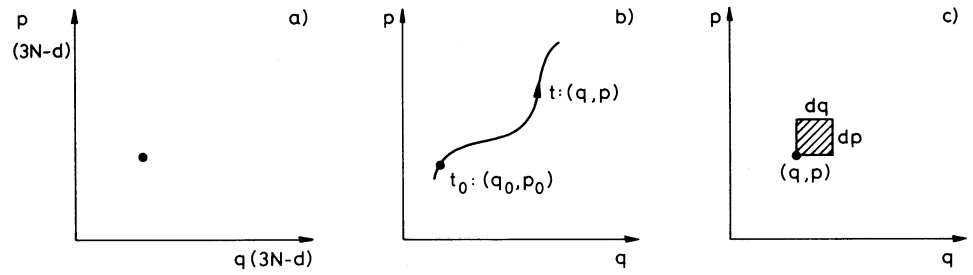

Figure 1: The 6N-dimensional phase space

Through specification of initial conditions, i.e., the 6N phase-space coordinates pertaining to the system at t=0, the 6N first-order differential equations (3) fix in a unique manner the phase-space trajectory, Fig. 1b.

In practice, N is a large number and there is a lack of complete information on the initial conditions. Consequently, a statistical description is introduced. We define a phase-space distribution $\varrho(q,p,t)$ such that

$$\varrho(q,p,t)dqdp \ , \qquad dqdp \equiv \prod_i dq_i dp_i \ , \tag{4}$$

gives the probability for finding the particle system within a volume dqdp near the point (q,p) at time t, Fig. 1c.

Liouville's theorem now states that: Provided solely Hamiltonian forces are acting, the phase-space density ϱ remains unchanged along a phase-space trajectory, i.e., ϱ is constant when measured at the variable position of a particle system moving through phase space, Fig. 2a. We may rephrase the theorem by stating that when $Q_i \equiv 0$, the volume enclosed by a given contour is conserved under the transformation (3), Fig. 2b.

In order to prove Liouville's theorem, consider a domain Ω in phase space, Fig. 2c. Due to continuity, the speed, by which the total probability for finding the particle system within Ω changes, equals the total influx of probability per unit time through $S(\Omega)$, the surface of Ω,

$$\frac{\partial}{\partial t} \int_{\Omega} \varrho \ dqdp = - \oint_{S(\Omega)} \vec{J} d\vec{S} \ , \qquad \vec{J} = \varrho \cdot (\dot{q},\dot{p}) \ . \tag{5}$$

Here, $\vec{J}$ is the 6N dimensional probability current density and $d\vec{S}$ is an outward directed surface element, $d\vec{S}=\hat{n}dS$. By means of the divergence theorem we may rewrite Eq. (5) as

$$\int_{\Omega} \left[\frac{\partial \varrho}{\partial t} + \sum_i \left(\frac{\partial}{\partial q_i} (\varrho \dot{q}_i) + \frac{\partial}{\partial p_i} (\varrho \dot{p}_i) \right) \right] dqdp = 0 \ . \tag{6}$$

Since Eq. (6) holds for any choice of Ω, the quantity in square brackets itself vanishes identically. By differentiation of the products and collection of the terms which contain derivatives of ϱ, we then obtain the relation

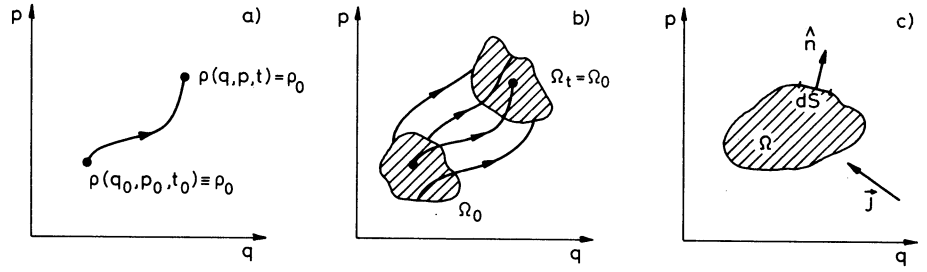

Figure 2: Liouville's theorem

$$\frac{d\varrho}{dt} = - \varrho \sum_i \left(\frac{\partial \dot{q}_i}{\partial q_i} + \frac{\partial \dot{p}_i}{\partial p_i}\right) . \tag{7}$$

When we now decide to follow the particle system in its motion through phase space, $\dot{p}_i$ and $\dot{q}_i$ are given by Eq. (3). Consequently, we arrive at the final result

$$\frac{d\varrho}{dt} = - \varrho \sum_i \frac{\partial Q_i}{\partial p_i} . \tag{8}$$

Evidently, if only Hamiltonian forces are acting, $Q_i \equiv 0$, the phase-space density remains constant, $d\varrho/dt \equiv 0$. This is the Liouville theorem. The relation (8) provides a generalization to cases where also non-Hamiltonian forces are acting, $Q_i \neq 0$.

It is worthwhile stressing at this point that interparticle forces are Hamiltonian as they are derivable from potentials like

$$U_{nm} = \frac{(Ze)^2}{|\vec{r}_n - \vec{r}_m|} , \qquad n \neq m , \tag{9}$$

where $\vec{r}_n$ denotes the position in direct space of particle number n. Consequently, in the 6N-dimensional phase space the introduction of interparticle interactions does not change the validity of the Liouville theorem as long as we do not consider inelastic processes like atomic excitation and ionization, charge transfer, or emission of radiation during collisions.

2.2 Reduction to 6 dimensions

The 6N-dimensional phase space is clearly not very suitable for practical purposes. Therefore, it is customary to introduce an alternative description based on 6 dimensions only, three spatial ones and three momentum coordinates. Each single particle of the system is represented by a point, Fig. 3a, so instead of one point in a 6N-dimensional space as in Fig. 1a we shall be working with N points in a 6-dimensional space. We introduce a particle density $f(\vec{q},\vec{p})$ in such a way that

$$dN = f(\vec{q},\vec{p}) d^3\vec{q} d^3\vec{p} \tag{10}$$

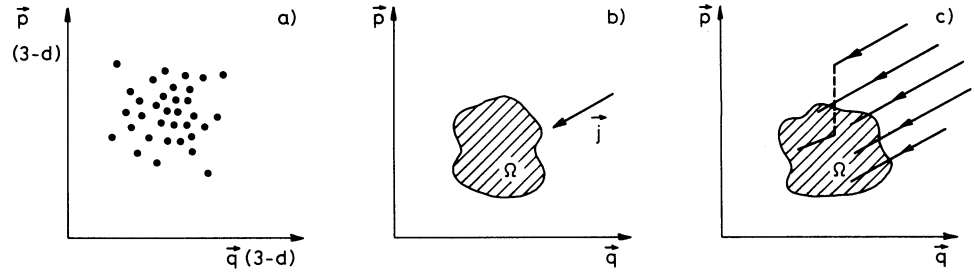

Figure 3: Distribution and motion in 6 dimensions

gives the number of particles within the volume $d^3\vec{q}, d^3\vec{p}$ around the phase-space point $(\vec{q},\vec{p})$. The basic question to be answered is then: What may be said about the evolution of f?

A formal reduction from 6N dimensions to 6 is described elsewhere [4,5]. We shall not embark on a discussion of this matter here. Instead, we shall be content by making a few simple observations. Consider first a situation where there is no inter-particle interaction. In this case, the single-particle Hamiltonian depends solely on $\vec{q}$ and $\vec{p}$ - and not on the phase-space coordinates $\vec{q}'$ and $\vec{p}'$ of other particles. Hence, the individual particle trajectories are independent and determined by the single-particle Hamiltonian $H(\vec{q},\vec{p})$ and, if active, by the non-conservative force $\vec{Q}(\vec{q},\vec{p})$. We may therefore repeat the continuity argument, Eq. (5), with f substituted for ϱ and a 6-dimensional current density of $\vec{j}=f\cdot(\dot{\vec{q}},\dot{\vec{p}})$, Fig. 3b. In analogy to Eq. (8) we obtain as a result

$$\frac{df}{dt} = - f \operatorname{div}_{\vec{p}} \vec{Q} \quad , \tag{11}$$

i.e., a 6-dimensional version of Liouville's theorem holds for $\vec{Q}\equiv 0$.

Allow now for interactions between the N particles. In this situation the 6-d continuity argument goes wrong! Besides streaming smoothly through the surface S(Q) of the phase-space volume according to the current density $\vec{j}$ (as determined by $H,\vec{Q}(\vec{q},\vec{p})$), Fig. 3b, there is the chance that a particle in its motion throughout phase space encounters closely another particle whereby it gets scattered, or kicked, into Q, Fig. 3c. We may therefore write

$$\frac{df}{dt} = - f \operatorname{div}_{\vec{p}} \vec{Q} + \left(\frac{\partial f}{\partial t}\right)_c \tag{12}$$

where the last term on the right-hand side symbolizes the change in f due to collisions. The "soft" part of the interparticle interaction, the collective "space charge" force due to all other particles, may be included in the single-particle Hamiltonian [4,5].

In the special case $\vec{Q}\equiv 0$, Eq. (12) takes in $(\vec{r},\vec{v})$-space the form

$$\frac{\partial f}{\partial t} + \vec{v}\,\frac{\partial f}{\partial \vec{r}} + \frac{1}{m}\left(\vec{F}_{ext} + \vec{F}_{sc}\right)\frac{\partial f}{\partial \vec{v}} = \left(\frac{\partial f}{\partial t}\right)_c \tag{13}$$

with $\vec{v}\equiv\dot{\vec{r}}$ and $\vec{F}_{ext}(\vec{r},\vec{v})$ denoting the external force. The space-charge force $\vec{F}_{sc}$ depends on

the distribution function $f(\vec{r},\vec{v})$ and thereby the equation (13) is seen to be highly non-linear. However, we stress that a 6-d version of the Liouville theorem holds even with inclusion of this interaction term provided only that the collision term $(\partial f/\partial t)_c$ may be neglected.

To see the significance of the collision term, consider the simple example of a free, neutralized, spatially homogeneous gas; $\vec{F}_{ext}=\vec{F}_{sc}=\partial f/\partial\vec{r}\equiv 0$. In this case Eq. (13) simply takes the form

$$\frac{\partial f}{\partial t} = \left(\frac{\partial f}{\partial t}\right)_c \quad . \tag{14}$$

If collisions are absent, f clearly remains unchanged relative to its initial value - which could be anything that does not depend explicitly on time. On the other hand, if collisions are present, the collision term assures that the distribution function relaxes towards thermal equilibrium. Natural questions, which appear in this context, are: How fast is the relaxation and what is the final equilibrium?

2.3 Evaluation of collision term

In order to answer questions on the trend towards equilibrium, we need an expression for the collision term. Our strategy is to adopt some physical model for collisions which links $(\partial f/\partial t)_c$ to $f(\vec{r},\vec{v})$.

Define $\psi(\vec{v},\Delta\vec{v})$ as the probability that a particle of velocity $\vec{v}$ acquires an increment $\Delta\vec{v}$ (due to collisions) within a time interval Δt. The value of the distribution function f in the phase-space point $(\vec{r},\vec{v})$ at time t may then be expressed in terms of the value of f in all points $(\vec{r},\vec{v}-\Delta\vec{v})$ at the slightly earlier time t-Δt as

$$f(\vec{r},\vec{v},t) = \int f(\vec{r},\vec{v}-\Delta\vec{v},t-\Delta t)\psi(\vec{v}-\Delta\vec{v},\Delta\vec{v})d^3\Delta\vec{v} \quad . \tag{15}$$

We note that the function ψ is assumed to be time-independent, the process is assumed to be a so-called Markoff process. Upon expansion of Eq. (15) to second order, the collision term takes the form[5)]

$$\begin{aligned}\left(\frac{\partial f}{\partial t}\right)_c &\equiv \frac{1}{\Delta t}\left(f(\vec{r},\vec{v},t) - f(\vec{r},\vec{v},t-\Delta t)\right) \\ &= \frac{1}{\Delta t}\left[-\sum_i \frac{\partial}{\partial v_i}\left(f\langle\Delta v_i\rangle\right) + \frac{1}{2}\sum_{ij}\frac{\partial^2}{\partial v_i\partial v_j}\left(f\langle\Delta v_i\Delta v_j\rangle\right)\right] ,\end{aligned} \tag{16}$$

with f evaluated in the phase-space point $(\vec{r},\vec{v})$. The symbol $\langle\ \rangle$ indicates an average over increments $\Delta\vec{v}$ with the weight function $\psi(\vec{v},\Delta\vec{v})$,

$$\langle\xi(\Delta\vec{v})\rangle \equiv \int\xi(\Delta\vec{v})\psi(\vec{v},\Delta\vec{v})d^3\Delta\vec{v} \quad . \tag{17}$$

Consequently, $\langle\Delta\vec{v}\rangle$ denotes the average velocity increment due to collisions within the time interval Δt, i.e., the quantity

$$\frac{m}{\Delta t}\langle\Delta\vec{v}\rangle \equiv \vec{F}(\vec{v}) \tag{18a}$$

may be interpreted as a dynamical friction force experienced by a particle penetrating the gas (of other particles) at velocity $\vec{v}$. Similarly,

$$\frac{1}{\Delta t}\langle \Delta v_i \Delta v_j \rangle \equiv D_{ij}(\vec{v}) \tag{18b}$$

are diffusion coefficients. Substitution of Eqs. (16) and (18) into Eq. (13) leads to the Fokker-Planck equation.

In a plasma, collisions involve in general many particles. However, in the following we shall assume that such multiple collisions may simply be treated as sequences of binary encounters. We sometimes refer to this picture as a binary-encounter model. Consider therefore two identical particles of velocities $\vec{v}_1$ and $\vec{v}_2$, charge Ze and mass m. We may describe their collision in the centre-of-mass system as the scattering through some angle θ of a particle (number 2) of velocity $\vec{w}\equiv\vec{v}_2-\vec{v}_1$ and mass m/2 on a fixed centre, Fig. 4. To determine the averages fixing the friction and diffusion coefficients, Eq. (18), we have to average over all scattering events involving a given 'test-particle' velocity, $\vec{v}\equiv\vec{v}_1$. The influx of particles (number 2's) amounts to $f(\vec{v}_2)w d\vec{v}_2$ $(cm^{-2}s^{-1})$ and with a cross section $d\sigma(w,\theta)$ for scattering into an element $d\Omega$ of solid angle we may write

$$\frac{1}{\Delta t}\langle \xi \rangle = \int d\vec{v}_2 d\Omega f(\vec{v}_2) w \frac{d\sigma(w,\theta)}{d\Omega}\xi \quad . \tag{19}$$

Eqs. (18) then take the form

$$\vec{F}(\vec{v}) = m\int d\vec{v}_2 d\Omega f(\vec{v}_2)|\vec{v}_2-\vec{v}| \frac{d\sigma(|\vec{v}_2-\vec{v}|,\theta)}{d\Omega}\Delta\vec{v}$$

$$D_{ij}(\vec{v}) = \int d\vec{v}_2 d\Omega f(\vec{v}_2)|\vec{v}_2-\vec{v}| \frac{d\sigma(|\vec{v}_2-\vec{v}|,\theta)}{d\Omega}\Delta v_i \Delta v_j \quad , \tag{20}$$

where the change in test-particle velocity depends on scattering angle and initial velocities, $\Delta\vec{v}=\Delta\vec{v}(\theta,\vec{v},\vec{v}_2)$.

To proceed, we need an expression for the differential scattering cross section. For pure Coulomb interaction, the Rutherford cross section applies, i.e.,

$$\frac{d\sigma}{d\Omega} = \frac{(Ze)^4}{m^2 w^4 \sin^4(\theta/2)} = \frac{d^2}{16\sin^4(\theta/2)} \quad , \tag{21}$$

where $d\equiv 4(Ze)^2/mw^2$ denotes the collision diameter. Upon insertion into Eq. (20) and integration over scattering angles, the friction and diffusion coefficients take the form

$$\vec{F}(\vec{v}) = \frac{8\pi(Ze)^4}{m} L \int d\vec{v}_2 f(\vec{v}_2) \frac{\vec{w}}{w^3} \quad ,$$

$$D_{ij}(\vec{v}) = \frac{4\pi(Ze)^4}{m^2} L \int d\vec{v}_2 f(\vec{v}_2) \frac{w^2\delta_{ij}-w_i w_j}{w^3} \quad . \tag{22}$$

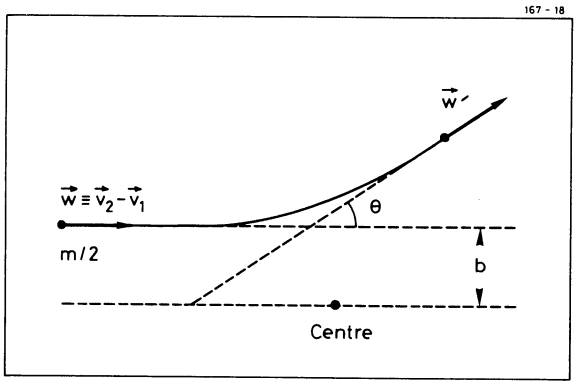

Figure 4: Diagram of binary collision

The "Coulomb logarithm" L is approximately given as $L \tilde{=} \ln(2/\theta_{min}) = \ln(2b_{max}/d)$, where θ_{min} denotes an effective minimum scattering angle corresponding to an effective maximum impact parameter b_{max}, which may result from, for example, screening by other ions in the gas or from the spatial extension of the gas container. Typically, L attains values of the order of 10 and its variation with w is thereby very slow. In consequence, L has been taken outside the integrals in (22). We leave it as an exercise for the reader to prove the relations (22). Ref. 5 or a similar textbook on plasma dynamics may be helpful.

2.4 Rates of diffusion

To estimate the rate of change of a non-equilibrium distribution $f(\vec{v})$ in its trend towards equilibrium, consider Eq. (16), which takes the form

$$\left(\frac{\partial f}{\partial t}\right)_c = -\frac{1}{m}\sum_i \frac{\partial}{\partial v_i}\left(f(\vec{v})F_i(\vec{v})\right) + \frac{1}{2}\sum_{ij}\frac{\partial^2}{\partial v_i \partial v_j}\left(f(\vec{v})D_{ij}(\vec{v})\right) \quad (23)$$

with the definitions (18). To characterize the distribution, let us compute various moments. The first moment defines the average value of the velocity $\vec{v}$, the second is related to the width of the distribution. To determine the n'th moment, multiply Eq. (23) through by v_x^n, where x signifies a fixed but otherwise arbitrary direction. Under the assumption that f vanishes rapidly at infinity, integration over all velocities (partial over v_x) yields for n=1,2 the results

$$\frac{\partial}{\partial t}\overline{v_x} = \frac{1}{m}\overline{F_x} \quad ,$$

$$\frac{\partial}{\partial t}\overline{v_x^2} = \frac{2}{m}\overline{F_x v_x} + \overline{D_{xx}} \quad , \quad (24)$$

where the bar indicates an average over the distribution function f,

$$\overline{\zeta(\vec{v})} = \int d\vec{v}\, f(\vec{v})\, \zeta(\vec{v}) \quad . \quad (25)$$

Note that f enters both in the averaging in Eqs. (24) and in the determination of the friction and diffusion coefficients.

Let us now pose the question: How quickly do particles immersed into the gas randomize? Or, in other words, how fast may we expect such particles to loose orientation? If we choose particles of the same type as the gas particles and with comparable speed, the answer clearly will provide information on the trend of the distribution $f(\vec{v})$ towards isotropy. Therefore, consider a single "test particle" of velocity $\vec{u}$, i.e., with a distribution function

$$f_t(\vec{v}) = \delta(\vec{v}-\vec{u}) \quad , \tag{26}$$

penetrating a "background" gas characterized by the usual distribution $f(\vec{r}_2,\vec{v}_2)$. The development with time of the test-particle distribution is governed by Eqs. (24), where the averages now are taken over f_t, whereas $\vec{F}$ and D_{ij} are determined by f. The first of Eqs. (24) determines the slowing-down on average of the test particle towards the "centre-of-gravity" of the gas distribution f. The second determines the noise or fluctuations in test-particle velocity acquired during slowing down. Randomization is inherent in this diffusion equation. To estimate the rate of loss of test-particle orientation, consider the blow-up of the square of the test-particle velocity in directions transverse to $\vec{u}$. With the distribution (26) inserted into the second of Eqs. (24), we obtain

$$\frac{\partial}{\partial t}\,\overline{v_\perp^2} = D_{\alpha\alpha}(\vec{u}) + D_{\beta\beta}(\vec{u}) \quad , \tag{27}$$

where α and β denote mutually perpendicular directions transverse to $\vec{u}$.

By means of the result (27), let us now estimate the time constant τ for relaxation towards isotropy for a few specific distributions $f(\vec{v})$. For a spatially uniform gas of density n and isotropical Maxwellian velocity distribution, the rate at which a test particle randomizes assumes the value

$$\tau^{-1} \equiv u^{-2}\,\frac{\partial}{\partial t}\,\overline{v_\perp^2} \simeq \frac{4\pi n(Ze)^4}{m^2}\,L\,\Delta^{-3} \tag{28}$$

when u is chosen as the root-mean-square velocity Δ of the gas (in one dimension) and the diffusion coefficients (22) are used. Ref. 5 or a similar textbook may be consulted during derivation of the relation (28). Alternatively, through introduction of a measure μ for the phase-space density of the gas, we may express the relaxation rate as

$$\tau^{-1} = 4\pi(Ze)^4 m\,L\,\mu \quad , \qquad \mu \equiv \frac{n}{m^3\Delta^3} \quad . \tag{29}$$

We prefer this representation when we later turn to the case of a beam. (Note that the actual phase-space density of the gas varies from point to point according to $f(\vec{v})$ - the quantity μ introduced in Eq. (29) only reflects the scale.)

Another example is that of a spatially uniform gas with an anisotropical Maxwellian velocity distribution,

$$f(\vec{r},\vec{v}) = nf(\vec{v}) = \frac{n}{\pi\sqrt{2\pi}\Delta_\perp^2\Delta_\parallel}\,e^{-(v_x^2+v_y^2)/\Delta_\perp^2}\,e^{-v_z^2/2\Delta_\parallel^2} \quad , \tag{30}$$

where we assume $\Delta_\parallel \ll \Delta_\perp$. To estimate the rate of relaxation towards isotropy of this distribution, take a test particle with a velocity in the disc of gas velocities, $\vec{u}=u\hat{x}$ with $u\tilde{<}\Delta_\perp$, and consider the diffusion to z-velocity space. This is determined by the coefficient $D_{zz}(\vec{u})=D_{zz}(u\hat{x})$. Clearly, the distribution (30) factorizes into a transverse and a longitudinal velocity distribution, $f(\vec{v})=f_z(v_z)f_\perp(v_\perp)$. A relevant quantity to compute would therefore be the blow-up rate for the longitudinal distribution,

$$\tau^{-1} \equiv \Delta_\parallel^{-2} \frac{\partial}{\partial t} \overline{v_z^2} = \Delta_\parallel^{-2} D_{zz}(u\hat{x}) \quad . \tag{31}$$

With the distribution (30) inserted into Eq. (22) we obtain, upon integration over all gas velocities, the result

$$\tau^{-1} \simeq 4\pi(Ze)^4 m\, L\, \mu \frac{\Delta_\perp}{\Delta_\parallel} \quad , \qquad \mu = \frac{n}{m^3 \Delta_\perp^2 \Delta_\parallel} \quad , \tag{32}$$

for $u\tilde{<}\Delta_\perp$, cf. the Appendix. Again, μ provides a measure of the phase-space density of the gas.

With this example, we close the discussion of the general description of relaxation towards isotropy of a non-equilibrium plasma. We are ready for the beam case!

3. SCATTERING WITHIN BEAM

3.1 What is special?

At first sight, the beam looks very different from the gas discussed above. However, if we transform away the drift $\vec{v}_0$ by working in a reference frame, the so-called particle frame (PF), which moves along with the average beam particle, scattering processes appear exactly as in the gas case. In particular, the motion in PF is non-relativistic and the scattering processes classical (i.e., non-quantal). The only complication to be encountered is that while the scattering naturally is described in physical space, the distribution functions, whose change we are interested in estimating (emittances, etc.), are given in a different set of generalized coordinates. In the accelerator we encounter couplings between the motion in x, y and z directions.

To illustrate the importance of such couplings, let us consider the following simple example, which is due to Derbenev [6]. At a given instant, two beam particles move transversely to the beam axis in PF in the horizontal plane at equal but opposite momenta, $\pm p_x$. Then, they perform a 90° collision whereby they are turned parallel to the beam axis, the momenta being conserved in magnitude. In the laboratory frame, the transverse components of the momenta of the two particles remain unchanged from their PF-values. However, the gain in longitudinal momentum during the collision, $\Delta p_\parallel$, is magnified by a factor of γ, where $\gamma \equiv (1-v_0^2/c^2)^{-1/2}$ is related to the total relativistic energy E of the average beam particle as $E=\gamma mc^2$. The situation is sketched in Fig. 5, for the laboratory

we have only shown the deviation in momentum from the average $\vec{p} \equiv \gamma m \vec{v}_0$. In PF, the sum of the momentum squares clearly is unchanged by the collision - the longitudinal blow-up is compensated by a transverse collapse. However, what happens to the single-particle emittances and $\Delta p/p$?

The collision illustrated in Fig. 5 leads to a growth in longitudinal phase space because, initially, the longitudinal momentum components vanished. Consider now the transverse phase space. For simplicity, we shall neglect derivatives of the lattice functions, $\beta' = D' \equiv 0$, whereby the horizontal (single-particle) emittance takes the form

$$\varepsilon_x = \frac{\pi}{\beta_x} \left[x_\beta^2 + \beta_x^2 \, x_\beta'^2 \right] \quad , \qquad x_\beta = x - D \, \frac{\Delta p}{p} \quad . \tag{33}$$

The physical point of scattering x remains unchanged by the collision. In terms of the betatron amplitude x_β and its derivative x_β', the scattering event is mapped by Table 1. Here the sign on terms containing p_x varies according to the particle considered. Insertion into Eq. (33) leads to a change of the sum of emittances for the two particles of

$$\Delta(\varepsilon_{x,1} + \varepsilon_{x,2}) = 2 \, \frac{\pi}{\beta_x} \left(\frac{p_x}{p} \right)^2 \left[(D\gamma)^2 - \beta_x^2 \right] \quad . \tag{34}$$

Evidently, the sign of the square-bracket factor in Eq. (34) decides whether the total emittance de- or increases. For $(D\gamma/\beta_x)^2 > 1$, we encounter simultaneous longitudinal and transverse growth!

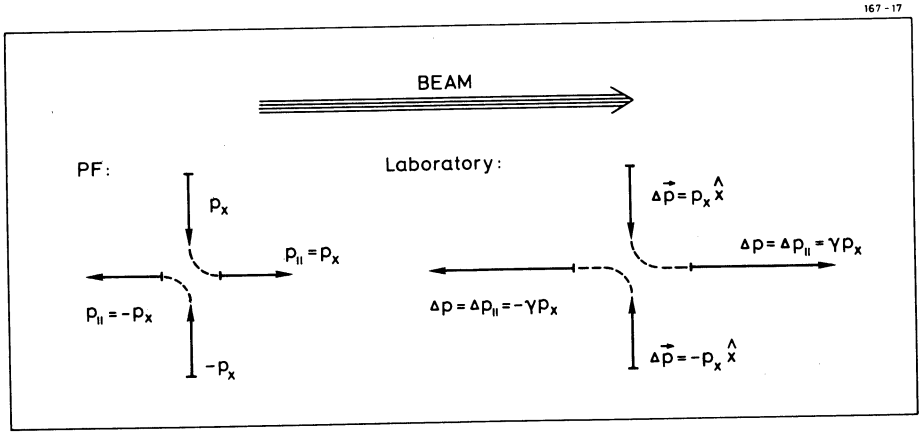

Figure 5: Sketch of Derbenev's collision of two beam particles

Table 1

Map of x_β and x_β' in Derbenev's collision

Time	x_β	x_β'
Before	x	$\pm \, p_x/p$
After	$x \mp D\gamma p_x/p$	0

3.2 Practical IBS calculation

Descriptions of practical calculations of intrabeam scattering (IBS) may be found elsewhere [1-2,7-8]. The classical reference is Piwinski's paper [1]. Here, derivatives of the lattice functions are neglected, which strongly limits the applicability. Improvements of Piwinski's treatment to account for the derivatives have been reported, for instance by Martini [2].

In general, the procedure used in the IBS-calculations is quite similar to that for the plasma case, Section 2, only are the formulas more complicated. We may sketch a typical calculation by the following succession of steps:

i) go to PF; here we have classical Rutherford scattering between pairs of identical particles;
ii) compute the change of single-particle emittances etc. (as defined in the laboratory frame) in a given binary (PF-) collision;
iii) assume simple phase-space distribution functions (Gaussians);
iv) average over all collisions (scattering angles, incidence and exit momenta, place of scattering).

These are the ingredients - practical performance is 'only' a question of technique!

Various IBS-computer codes are available on the market. Inputs are storage-ring lattice and beam (type and number of particles, momentum, emittances and $\Delta p/p$) and the output consists of heating rates for vertical and horizontal emittances and longitudinal momentum spread. We advocate Martini's version since this is written in a transparent way and appears well documented [2,9].

3.3 Examples of IBS rates

Rather than dwell on technical details of the IBS-calculations, let us play around a bit with some of the available computer codes. In doing so, the question immediately appears how to represent the data in a reasonably compact manner?

Let us for a moment assume that the velocity distribution of the beam in PF is a Maxwellian and the spatial density a constant. In this case the diffusion rate in PF is defined by Eq. (29). To transform to the laboratory frame, we note that the spatial density n and the longitudinal momentum spread $\Delta p_{\parallel}$ is magnified by a factor of γ, whereas the transverse component of the momentum $p_{\perp}$ is unaffected upon transformation. This leads to a conserved phase-space density,

$$\left.\begin{aligned} n^{L} &= \gamma n^{PF} \\ \Delta p_{\parallel}^{L} &= \gamma p_{\parallel}^{PF} \\ p_{\perp}^{L} &= p_{\perp}^{PF} \end{aligned}\right\} \quad \Longrightarrow \quad \mu^{L} = \mu^{PF} \quad . \tag{35a}$$

Accounting for time dilation

$$\tau^{L} = \gamma \tau^{PF} \quad , \tag{35b}$$

we obtain for the Maxwellian PF-distribution a rate of

$$\tau_L^{-1} = \gamma^{-1}\, 4\pi (Ze)^4 m\, \mu\, L \quad . \tag{36}$$

To represent IBS-data for a realistic beam, our first suggestion could therefore be to plot $\tau^{-1}\gamma/\mu$ or, rather, $(\Sigma\tau^{-1})\gamma/\mu$ as a function of emittance and longitudinal momentum spread. Here, the summation sign indicates the sum over blow-up rates for horizontal and vertical emittances and longitudinal momentum spread, $\Sigma\tau^{-1} \equiv \tau_H^{-1} + \tau_V^{-1} + \tau_p^{-1}$.

Figure 6 shows examples of such plots for coasting proton beams of equal horizontal and vertical emittances circulating in two different CERN storage rings, the former ICE-ring (γ_t=1.3) at p=0.3GeV/c and LEAR (γ_t^2=-(14.5)^2) at p=0.6GeV/c. For ICE we have used Martini's code, for LEAR a code written by Möhl [10]. Corrections have not been made for the slightly different definitions of beam emittances and $\Delta p/p$ (relations to widths of Gaussians) applied in the two programs. For the measure μ of the phase-space density entering the ordinate in Fig. 6, we have substituted the expression

$$\mu^{-1} = N^{-1} p^3 \varepsilon_H \varepsilon_V C \Delta p/p \quad , \tag{37}$$

where N denotes the total number of beam particles and C is the circumference of the ring in question; our unit of emittance is πmrad, of momentum GeV/c and of length and time m and sec, respectively. Note that only the points are calculated - curves are drawn to 'guide the eye'.

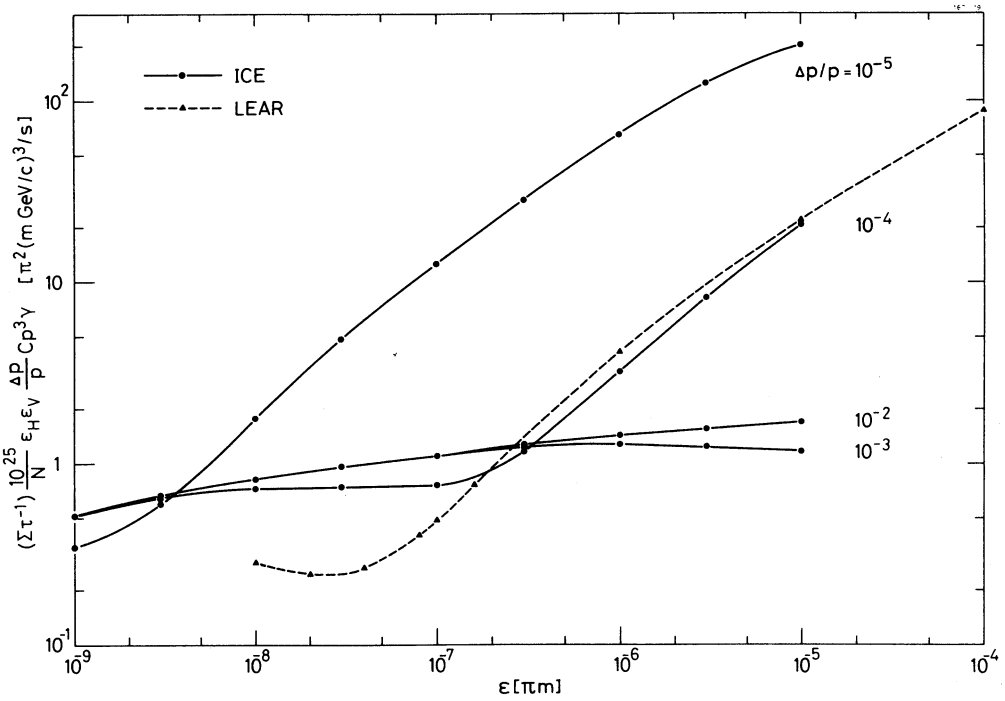

Figure 6: Intrabeam scattering in ICE and LEAR

Let us stress some of the main observations to be made from Fig. 6: First of all, we note that there is always growth, i.e., the ordinate in the figure is always positive (the individual blow-up or 'heating' rates may be negative as well as positive). This implies that, in general, the beam never reaches an equilibrium. Secondly, we encounter for any fixed value of $\Delta p/p$ a smooth behaviour, that is, a slow increase in the normalized rate with increasing emittance up to a certain point where a more rapid dependence sets in. To the left of the point (the flat portion of the curve) the blow-up rate is dominated by τ_H^{-1}, to the right (steep portion of the curve) τ_p^{-1} dominates. Throughout, τ_V^{-1} plays a minor rôle. Thirdly, the break-up point is positioned exactly in the region where coupling in the horizontal plane becomes important. Since the (Gaussian) width of the beam in this direction is composed by two contributions, one, $\sigma_{H\beta}$, which is due to betatron oscillation and another, $D\sigma_p$, which appears because of the coupling via the dispersion to the momentum spread σ_p, that is, since

$$\sigma_H^2 = \sigma_{H\beta}^2 + D^2\sigma_p^2 \quad , \tag{38}$$

the point in question appears for $\sigma_{H\beta}^2 \sim D^2\sigma_p^2$ or, equivalently, for

$$\varepsilon_H \sim \langle \frac{D^2}{\beta_H} \rangle \, (\frac{\Delta p}{p})^2 \quad . \tag{39}$$

A typical value for the average $\langle\ \rangle$ around the storage ring of D^2/β_H could be in the range 1-10m. Finally, the patterns observed for different machines are similar.

3.4 Representation of IBS-data by reduced variables

The study of Fig. 6 immediately suggests further condensation of the IBS-data by plotting the curves as functions of the reduced variable $\varepsilon/(\Delta p/p)^2$, cf. Eq. (39). The only question which remains is then what the optimal choice for the second axis may be? To the right of the break-up (or, perhaps, "break-even") point, couplings between the three planes of motion may be neglected. In the same region, the beam has collapsed longitudinally in momentum space, in PF even with an additional factor of γ. Consequently, the steep portion of the curve corresponds to a PF-rate similar to (32). Transformation to the laboratory frame proceeds via Eqs. (35). Since the phase-space density is conserved, while the γ-factors from time dilation and longitudinal momentum spread cancel, we obtain

$$\tau_L^{-1} \simeq 4\pi(Ze)^4 m\mu L \left[\frac{\langle p_\perp^2 \rangle}{\langle \Delta p_\parallel^2 \rangle} \right]_L^{1/2} \propto Z^4 m\mu L \, \frac{\sqrt{\varepsilon}}{\Delta p/p} \quad , \tag{40}$$

which is independent of γ.

Biased by the result (40), we show in Fig. 7 a plot of $(\Sigma\tau^{-1})\mu^{-1}\langle L\rangle^{-1}$ as a function of $\varepsilon/(\Delta p/p)^2$ for a coasting proton beam circulating in ICE. The conditions are the same as in Fig. 6 and for μ we have again substituted the measure (37). Through the points computed for $\Delta p/p = 10^{-4}$ we have drawn a curve to guide the eye. To our great satisfaction we observe that the normalized rates corresponding to the three remaining ICE-curves of Fig. 6 fall very close to the 10^{-4} curve. For the storage ring given, the intrabeam

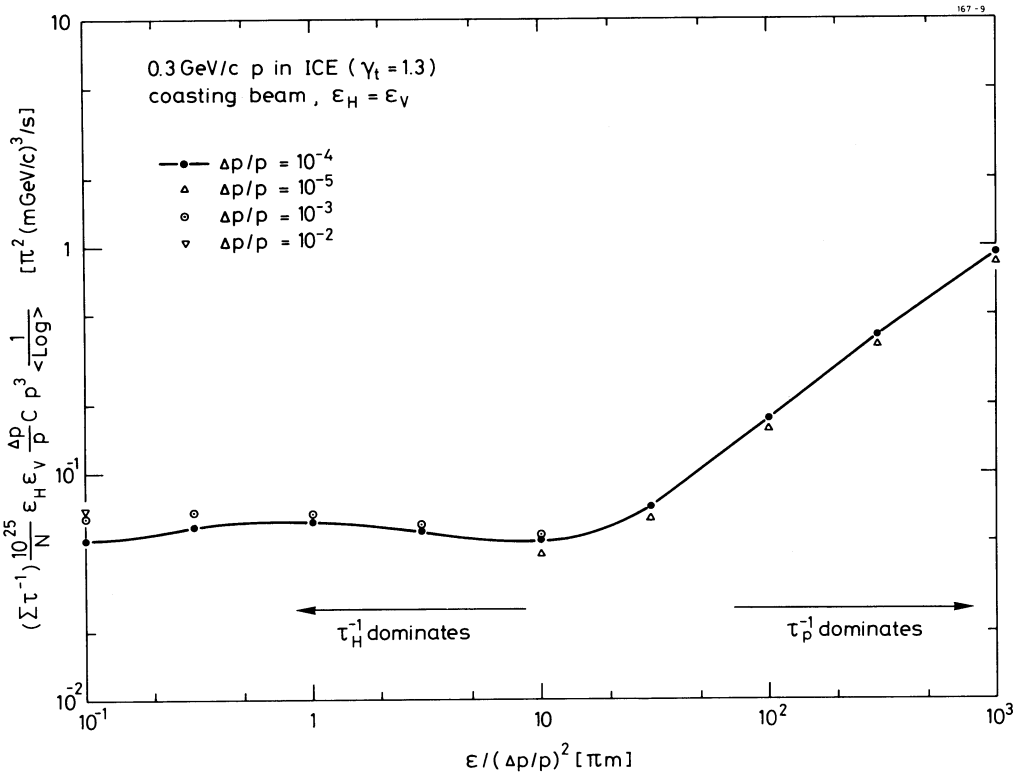

Figure 7: IBS-rates for ICE in reduced variables

scattering may to a very good approximation be represented by a single universal curve! Scaling to particles of different charge and mass is straightforward, cf. expressions like (36) and (40). It may be noted that to obtain a single curve with as high accuracy as in Fig. 7, it is essential to include in the ordinate the average $\langle L\rangle$ around the ring of the Coulomb logarithm.

The patterns observed for other storage rings - from the low-energy ring ASTRID in Aarhus to the high-energy antiproton accumulator at Fermilab - are quite similar to the ICE case shown in Fig. 7. Even the absolute numbers are similar, indeed, we have never for any lattice tested encountered normalized rates which have been more than approximately a factor of four off the curve displayed in Fig. 7. To the right of the break-up point, the agreement is even within a factor of two.

Clearly, one may think of rescaling once more the IBS results for the purpose of producing a universal curve which could represent the data obtained with any given lattice. The first one could imagine to do could be, for example, to include in the horizontal scale a factor of $\langle D^2/\beta_H\rangle^{-1}$ to account for the variation in the break-up point, Eq. (39). Next, one could consider if the phase-space measure μ is expressed in a sufficiently machine-independent manner by Eq. (37). Also the dependence of the constant of proportionality in the last relation in Eq. (40) on lattice parameters should be considered. Whether further rescaling could be successful appears doubtful, however. It is clear that while the steep part of the curve in Fig. 7 has a simple interpretation, Eq.

(40), the flat part is strongly dominated by the couplings in the transverse plane, i.e., we shall expect this part of the curve to be more machine-dependent than the former. Our recommendation should therefore be: For the lattice of interest, compute once and for all the universal curve, cf. Fig. 7, and trust this within typically 50%.

4. CONCLUDING REMARKS

Through the previous paragraphs we have intended to give a transparent introduction to the phenomenon of intrabeam scattering. We have emphasized the close analogy between IBS and the trend towards isotropy in velocity space of a plasma and, at the same time, stressed the differences which are due to the couplings of the degrees of freedom in the accelerator. Rather than going through all the technical details of IBS calculations, we have chosen to show results of numerically computed rates. A study of such data, combined with the general considerations for the plasma case, led to the production of a strongly reduced representation of IBS-rates: For a given lattice a single, universal curve may be created, which allows for a quick read-off of heating rates in any situation. Furthermore, the universal curves corresponding to even very different machines (as far as tested) differ by less than an order of magnitude.

Finally, let us mention that a few experimental measurements of IBS heating rates exist. These all seem to agree with the results obtained from the computer codes, cf. Refs. 2 and 7.

ACKNOWLEDGEMENT

The author wishes to thank S.P. Møller for stimulating discussions.

REFERENCES

1) A. Piwinski, Proc. CERN Accelerator School on General Accelerator Physics, Gif-sur-Yvette, Paris, 1984 (CERN 85-19, CERN, Geneva, 1985) 451-462; this contribution is essentially identical to the original paper published in Proc. 9th Int.Conf. on High Energy Accelerators, 1974.

2) M. Martini, CERN PS/84-9(AA) (1984).

3) H. Goldstein: Classical Mechanics (Addison-Wesley, Reading MA, 1957).

4) A.J. Lichtenberg: Phase-Space Dynamics of Particles (Wiley, New York, 1969).

5) T.J.M. Boyd and J.J. Sanderson: Plasma Dynamics (Nelson, London, 1969).

6) Ya.S. Derbenev, Fermilab $\bar{p}$-Note 176 (1981).

7) M. Conte and M. Martini, Part.Acc. 17 (1985) 1.

8) J.D. Bjorken and S.K. Mtingwa, Part.Acc. 13 (1983) 115.

9) M. Martini, PS/AA/Note 84-7 (1984).

10) D. Möhl (unpublished).

11) M. Abramowitz and I.A. Stegun: Handbook of Mathematical Functions (Dover, New York, 1972).

APPENDIX

In order to derive the expression (32) for the blow-up rate in the axial direction of a flattened Maxwellian velocity distribution, Eq. (30), we need an expression for D_{zz}, cf. Eq. (31). With a transverse test-particle velocity, $\vec{u}=u\hat{x}$, this component of the diffusion tensor reads

$$D_{zz} = \frac{4\pi n(Ze)^4}{m^2} L \int d^3\vec{v}\, f(\vec{v}) \frac{w^2-w_z^2}{w^3} , \qquad \vec{w} = \vec{v} - u\hat{x} , \qquad (A1)$$

according to Eq. (22). A change of integration variable gives

$$D_{zz} = \frac{4n(Ze)^4}{\sqrt{2\pi}m^2\Delta_\perp^2\Delta_\parallel} L \int d^2\vec{w}_\perp dw_z \frac{\vec{w}_\perp^2}{w^3} e^{-(\vec{w}_\perp+u\hat{x})^2/\Delta_\perp^2} e^{-w_z^2/2\Delta_\parallel^2} , \qquad (A2)$$

where $\vec{w}_\perp$ and $w_z\hat{z}$ denote the components of the relative velocity transverse and parallel to the axis, respectively. When the velocity distribution is assumed excessively flattened, $\Delta_\parallel << \Delta_\perp$, the factor w^{-3} may be replaced by $w_\perp^{-3}$. The diffusion coefficient (A2) then reduces to

$$D_{zz} = \frac{4n(Ze)^4}{m^2\Delta_\perp^2} L \int_0^\infty dw_\perp e^{-(w_\perp^2+u^2)/\Delta_\perp^2} \int_0^{2\pi} d\varphi\, e^{-2w_\perp u\cos\varphi/\Delta_\perp^2} . \qquad (A3)$$

Integration over the azimuthal angle φ yields the modified Bessel function I_0,

$$D_{zz} = \frac{8\pi n(Ze)^4}{m^2\Delta_\perp^2} L \int_0^\infty dw_\perp e^{-(w_\perp^2+u^2)/\Delta_\perp^2} I_0\left(\frac{2w_\perp u}{\Delta_\perp^2}\right) , \qquad (A4)$$

cf. Ref. 11. In turn, the $w_\perp$ integration may be performed to give[11]

$$D_{zz} = \frac{4\pi n(Ze)^4}{m^2\Delta_\perp} \sqrt{\pi}\, e^{-u^2/2\Delta_\perp^2} I_0\left(\frac{u^2}{2\Delta_\perp^2}\right) . \qquad (A5)$$

The function $e^{-x}I_0(x)$ decreases slowly with x; at x=0 it equals 1, for $x>>1$ it approaches $(2\pi x)^{-1/2}$ and for $x\approx\frac{1}{2}$ we have $\sqrt{\pi}\, e^{-x}I_0(x)\simeq 1$ (Ref. 11). In consequence, we may write

$$D_{zz}(u\hat{x}) \simeq \frac{4\pi n(Ze)^4}{m^2\Delta_\perp} L , \qquad u \simeq \Delta_\perp . \qquad (A6)$$

Insertion of this result into Eq. (31) leads to the rate (32).